Reassembling a traveling-wave Stark decelerator and testing its performance

Hidde H. Makaske
s2745399
1 November 2019

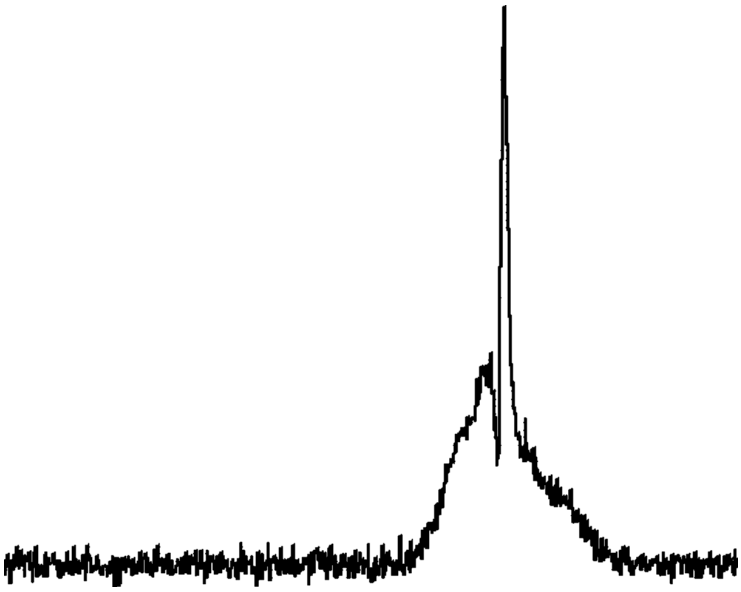

First supervisor: prof. dr. S. Hoekstra
Second supervisor: prof. dr. ir. P.R. Onck

university of groningen / faculty of science and engineering / van swinderen institute for particle physics and gravity

Abstract

To investigate beyond the standard model physics the NL-eEDM collaboration will perform a measurement on the electric dipole moment of the electron using BaF molecules. In order to achieve a high precision on this measurement multiple stages will be used to prepare these BaF molecules for this measurement. In one of these stages a traveling-wave Stark decelerator will be used to slow down these molecules.
In this thesis the process of reassembling and upgrading of this decelerator for the experiment is documented. Possible decreases in performance due to misalignment are investigated with simulations. And its performance is investigated after it was coupled to a cryogenic source.

Contents

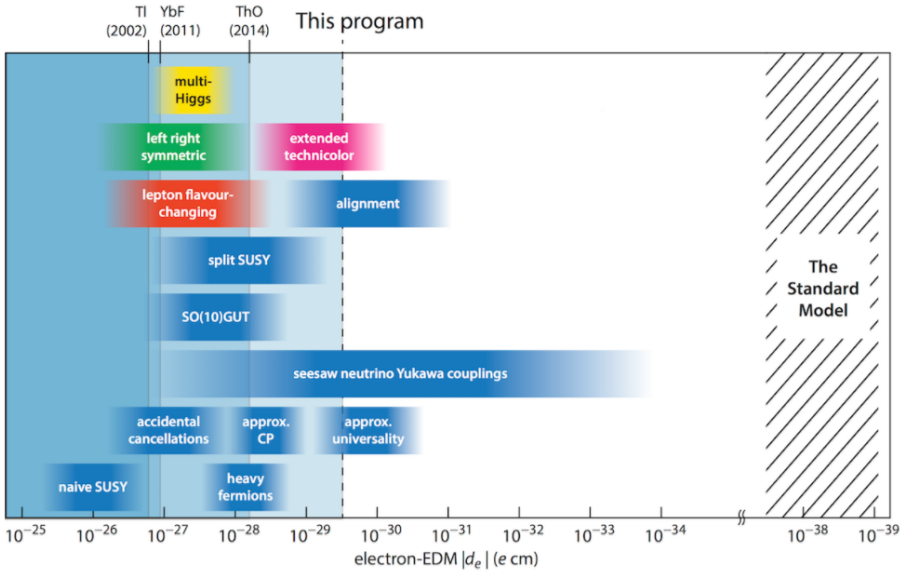

Figure 1: Different predictions of the eEDM from different BSM theories, the dashed line is the proposed precision by the nl-eEDM collaboration

1 Introduction

1.1 The electron Electric Dipole Moment

The Standard Model (SM) of Particle Physics has been proven over the years to be a very successful theory in the sense that it was able to describe experimental outcomes to a very high precision. However, there are also some parts that are incomplete and flaws in the theory. The SM for example, does not include gravity and is not able to explain the matter- antimatter asymmetry in our universe adequately. In order to come to a better theory without losing the great achievements of the SM, some theoretical physicists try to make extension to the SM, so-called beyond the Standard Model physics (BSM).
BSM theories often predict additional mechanisms which would solve some of the current issues with the SM. But these mechanisms would cause deviations of certain fundamental constants. One such fundamental constant is the electron's Electric Dipole Moment (eEDM) [1]. As can be seen from figure 1, the predicted value of the eEDM by the SM is eight orders of magnitude lower than several BSM predictions. From an experimental point of view, it is impossible to detect such a small eEDM given the current state of the available technology. However state of the art experiments could potentially lower the upper limit on the value of the eEDM. The current limit set by the ACME II collaboration is $|d_e| < 1.1 \cdot 10^{-29} e \cdot cm$ with a 90 % confidence level [2]. Lowering this value puts stringent requirements on BSM theories but finding an eEDM would cor-

roborate the theories that predict an eEDM of that order of magnitude.
The eEDM would arise from an a-spherical distribution of the charge of the electron alongside the direction of the spin. This eEDM would violate T-symmetry and CP-symmetry, assuming that, CPT symmetry holds [3]. Questions regarding CP-violation are directly connected to the matter/anti-matter asymmetry in the universe.

1.2 The NL-*e*EDM collaboration

The NL-eEDM collaboration has the goal to lower the upper limit on value of the eEDM to $d_e = 5 \cdot (10^{-30} e \cdot cm)$ [4]. To achieve such precise measurements molecules are used. In the case of the NL-eEDM collaboration, BaF molecules are used.
To measure the eEDM, BaF molecules are put in a hyperfine superposition state via a $\pi/2$ pulse. The molecules then travel through an interaction zone, in which electric fields and magnetic fields can be generated. Where the electric field is either parallel or anti-parallel to the direction of the magnetic field. In this interaction zone, a phase is accumulated. By then again applying a $\pi/2$ pulse, and subsequently using a fluorescence detection setup, it is possible to measure this accumulated phase.
In the absence of an eEDM the accumulated phase of the molecule travelling parallel to these lab fields would be the same as the accumulated phase when the molecules travel anti-parallel to the lab fields. However, in the case of an existing eEDM the there would be a difference between both cases. This phase difference would be proportional to the eEDM. The statistical error on such a measurement is given

$$\sigma_{stat} = \frac{\hbar}{2|P|E_{\text{eff}}\tau\sqrt{\dot{N}T}}, \tag{1}$$

where P is the degree of polarisation, E_{eff} is the effective electric field that the valence electron experience. This is high for the valence electron on BaF, which has a value of 6-8.5 GV/cm and is determined numerically. τ is the coherent time for which the phase is accumulated. Essentially meaning the time that the molecules spent in the interaction zone. $\dot{N}$ is the number of detected molecules per unit time and T is the total measurement time.
In order to minimise the statistical uncertainty on the measurement it is important to maximise τ and $\dot{N}$. In order to meet these requirements the NL-eEDM collaboration proposed a setup shown in figure 2.
The BaF molecules necessary for the experiment are created in the cryogenic source. This source produces cold BaF molecules at a 10 Hz frequency. The mean velocity of such a beam is 200 m/s. The guide is an electrostatic trap that leads the molecules towards the decelerator reducing transverse losses. The decelerator is a travelling-wave Stark decelerator (TWSD). It uses the Stark effect to slow down the molecules in the longitudinal direction, which will improve the interaction time, for the time spent inside the interaction zone increases. This

is then followed up by a laser cooling section which cools the molecules in the transverse direction which also helps to increase the coherent interaction time. Recently there has been some development regarding using triatomic molecules for these kind of experiments. For more information on this see Appendix A or the thesis of K. Steinebach [5].

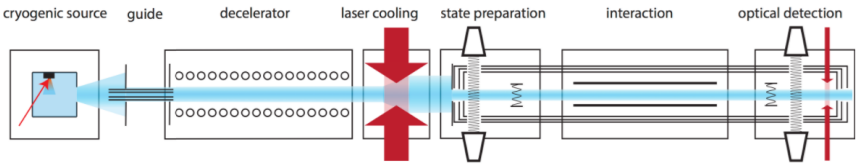

Figure 2: A schematic drawing of the eEDM measurement setup

1.3 This thesis

In section 2 the travelling-wave Stark decelerator is described, its working principles and the technical implementation.
The present decelerator does not yet meet all the requirements for NL-eEDM. In order to prepare the decelerator for this experiment it is decided to disassemble the decelerator. Section 3 reports on the methods used to reassemble the TWSD and the achieved precision of the realignment will be given.
Simulations to quantify the performance of the newly aligned TWSD will be performed in section 4. The goal of the simulations is to quantify the reduced efficiency of the decelerator due to misalignments.
In section 5 it is investigated if the newly obtained experimental data can be compared with the previously obtained experimental data. The new experimental data being the data obtained from the TWSD in combination with a cryogenic source. And the previous data is the data that was gathered from the TWSD in combination with a supersonic source. This comparison could give information about the efficiency of the reassembled decelerator.
In section 6 we will try to extract information on the performance of the decelerator by comparing the experimental data with simulated data.

2 Slowing down BaF using a travelling wave Stark decelerator

In this section an investigation is undertaken into how the traveling-wave Stark decelerator uses electric fields to slow down neutral BaF molecules.

2.1 The BaF molecule in an electric field

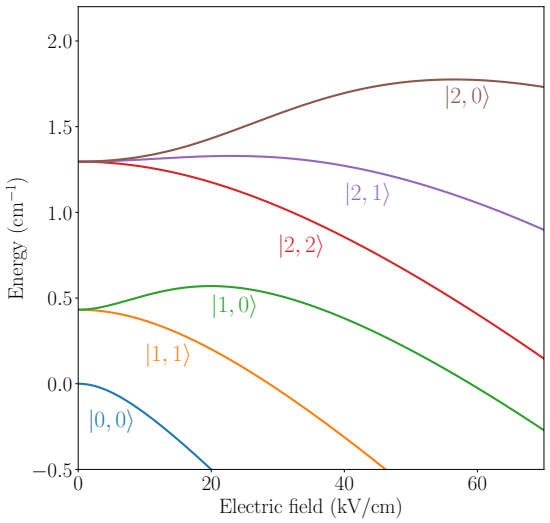

Figure 3: The Stark Curves for BaF, $|N, M_n\rangle$ where N is the rotational number, and M_n is its projection on the the electric field. The labelling is on the basis of their zero field quantum numbers. The $|2,0\rangle$ state is for example a lfs for voltages under 50 kV/cm [5]

When an atom or molecule is placed in an electric field the Stark effect occurs [6, 7]. The Stark effect causes the mixing of the different rotational states and their projections of the rotational quantum number on the electric field axis, thus changing the basis set of the Schrödinger equation. This mixing leads to an induced dipole moment in the lab frame, and at a high electric field the only good quantum number is the projection M_n on the electric field. This results in a shift in energy of different states for different voltages. These so-called Stark curves for BaF are given in figure 3.
It holds that there is a force $\mathbf{F}$ for which hold: $\mathbf{F} = -\nabla\mathbf{E}(\mathcal{E})$ where $\mathcal{E}$ is the electric field. From figure 3 it can be found that for some states a lower electric field leads to a lower energy. So in a non-uniform electric field the molecules at those states, at the right electric field strength, will "roll down" to these region with lower electric field. For that reason we call these states low field seeking states (lfs). All the other states are called high field seeking states (hfs), for the

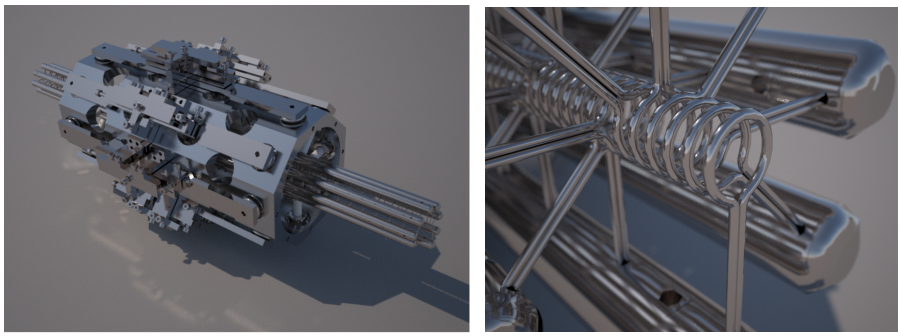

(a) (b)

Figure 4: (a) A drawing of one module. (b) A zoom-in on the the electrodes which are connected to the rods.

obvious reason that they experience a force in the direction of the electric field gradient.

2.2 The travelling-wave Stark decelerator

Using the concepts of lfs and hfs states we can manipulate the motion of the molecules using electric fields. By the laws of Maxwell it is impossible to create a maximum of an electric field in free space. It is, however, possible to create an electric field minimum in free space. For that reason the lfs molecules are of interest in our experiment. Essentially the TWSD will slow down the BaF by manipulating electric fields which are seen as potential wells by the BaF molecules.

2.2.1 The mechanical construction of the decelerator

The decelerator was originally built out of 9 modules, one of these modules is shown in figure 4a. Each module is 500 mm long and this results in a decelerator with a length of 4.5 m in total. In every module there are eighth rods and on every rod there are 42 electrode rings with an inner diameter of 4.0 mm, some of these electrodes are shown in figure 4b. The rods in a modules are shifted 1.5 mm between each other such that a periodic structure of electrodes occurs. The electrodes demarcate a "tube" through which the molecules will flow, as is visible in figure 4a.
Pairs of two modules are put upon a rail system shown in figure 5. This rails are mechanically connected to the vacuum chamber by an adjustment system called the hat. The ninth module was connected via a different custom construction.

Rods which have the same place on different modules are electrically connected. Thus by applying a voltage to one of the rods a periodic electric field throughout this tube can be created. By applying a sinusoidal voltage to all the rods with

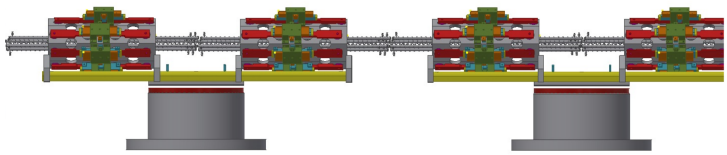

Figure 5: A schematic drawing of the rail system. It shows 2 hat adjustment system, both supporting a rails, each piece of rails carries 2 modules

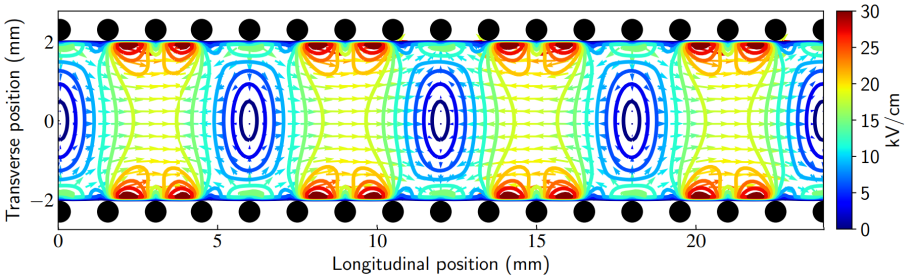

Figure 6: The electric field within the decelerator, it is periodic every 6 mm [8]

a phase difference of $\frac{2\pi}{8}$ between each consecutive rod, travelling minima with a periodicity of 6 mm are created shown in figure 6. The speed of these minimums is determined via with the frequency of the sinusoidal voltage as

$$v(t) = 12mm \cdot \omega(t), \tag{2}$$

where ω is the frequency of the voltage amplitude. The voltage on n-th rod will be described as

$$V_n(t) = V_a \sin\left(-\frac{2\pi}{12mm}\int_0^t v(\tau)d\tau + \frac{2\pi n}{n}\right) \tag{3}$$

where V_a is the voltage amplitude, and $v(t)$ is the velocity of the trap at time t [8].
During experiments the rods are connected to high voltage amplifiers that deliver a sinusoidal voltage. They deliver that voltage only for a limited time per molecular packet.

2.2.2 Slowing down molecules

The TWSD allows for a precise control of the periodic electric fields minima within a line concentric with the centre of the circular electrodes. These minima act as potential wells for the lfs molecules. In order to slow down the molecules the velocity of the travelling traps can be slowed down. By slowing down the

trap the molecule gains velocity with respect to the trap and thus shifts to a region with a higher electric field. It then experiences a force that pushes it back to a lower electric field value which is again the centre of the trap, effectively slowing down the molecule in the longitudinal direction. By slowing down the traps gradually you can slow down the molecules as well as it experiences a force towards the centre of the trap which is net slower. This slowing down has to be done gradually otherwise the velocity that the molecule gains w.r.t. the trap becomes large enough to escape the trap potential.
In order to quantify the trap depth we can plot a separatrix. A separatrix is essentially the solution to the question: "What is the escape velocity of the molecule at a certain position in the trap in one dimension?". So, in other words, all the molecules that fit inside all the different seperatices are eligible to be slowed down. This is dependent on the specific Stark curve of the molecular state and the voltage applied to the rings. In the case of deceleration, the separatrix becomes smaller and asymmetric, as is shown in figure 7a.
One of the unique features of the TWSD, compared to other molecule slowers, is that it not only traps in the longitudinal direction but it also traps transversely. This greatly reduces possible losses through these channels and allows for long decelerators a typical transverse separatrix is shown in figure 7b.

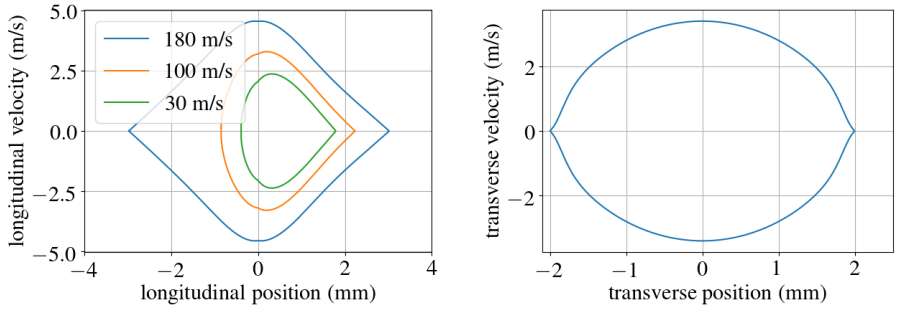

(a) (b)

Figure 7: By simulating the energy potential within the decelerator operating at 5 kV for BaF(1,0) following separatrices were made: (a) The longitudinal separatrix for different deceleration strengths, starting from 180 m/s going to the velocities indicated in the legend. For higher deceleration strengths the area becomes smaller. These seperatices are taken with a radial component of zero. (b) The transverse separatrix of the decelerator at the at the centre of the trap. Molecules with a transverse velocity higher than 3 m/s will not be trappable by the decelerator, in this case.

3 Rebuilding a 4 meter long decelerator

The 4.5m long decelerator was built for another experiment, and in order to prepare it for the eEDM experiment some changes and upgrades had to be made. It was decided that, to properly upgrade the decelerator it had to be dissembled completely, apart from the vacuum chamber. This was done for multiple reasons. Firstly, it was decided, that the cryogenic source would be positioned on the former position of the laser-induced fluorescence (LIF) setup. For a good coupling of the source to the decelerator, the central line of the the alignment of the decelerator had to be in the middle of the vacuumchamber, at the position of the coupling. This was not the case in the previous setup. Secondly, there was also reason to believe that realigning the device could improve its performance, as there was kink between different modules. A third reason had to do with the electrical connections between rods of different modules which would not function properly at the higher voltages needed for the NL-eEDM experiment.

3.1 Realignment

The decelerator was built over the course of a few years. Several times over the years, modules were added for a more efficient deceleration. Due to more expertise the modules appended at later stages were better aligned than ones appended at the early stages. This way of constructing the apparatus in phases caused a little kink in the global path that the electrodes traced out. This prohibited the possibility to look through all the electrodes simultaneously.
After the decelerator was taken apart, alignment started in different stages: first the individual electrodes on the rods were aligned; then the rods were aligned w.r.t. each other inside a module; and finally the rails inside the vacuumchamber was aligned such that the modules could be placed properly. During all these stages of alignment data was gathered regarding the precision of the alignment, something which was not available to such an extent previously. The tables regarding that precision are shown in section 3.1.5.

3.1.1 Alignment of the electrodes on a rod

A schematic figure of the different sources of misalignment of the electrodes on the rods is shown in figure 8. The bend was checked in the transverse direction θ, by putting the the rod upon a surface table, that is flat within 0.005 mm. Using small metal plates, the deviations were determined. Corrections of these errors were performed manually. The error was limited to 2 mrad or 0.05 mm. The bending in longitudinal direction, ϕ, was checked by putting the rod on a 'manual vision measuring machine' from Mitutoyo. Whenever the bend exceeded an error of 3 mrad the angle would be corrected. There were no explicit tests on ω, which is the amount of twist in the rods, however during the stage involving the Mitutoyo device some deviation were found and were corrected manually when possible . From visual inspection the deviation was typically within 40 mrad. Errors in the length L and the radius R were also

not explicitly tested but seemed to be in agreement with the values given by the dissertation of van den Berg [9].
Most of the deviations were found in the rods from the modules from the earlier generations of the experiment. The more recent modules did not need a lot of treatment, and for some modules of the newer generations it was assumed that the rods were within our error margins.

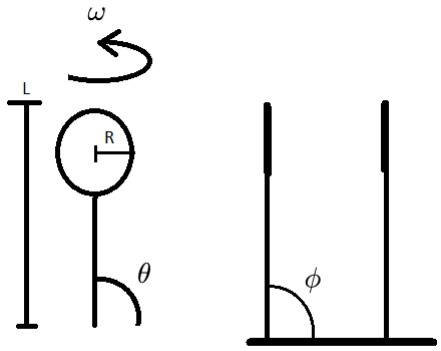

Figure 8: On the left side there is a frontview of a single electrode, on the right side there is a side view of two electrodes

3.1.2 Alignment of rods within a module

It is possible to make a distinction between two phases in this stage of alignment: the transverse alignment e.g. the overlap between the rings in one module; and the longitudinal alignment, which can be seen as setting the proper distance between the rings.

Transverse alignment
In order to align rods withing the modules the following setup is used (see figure 9). A small set of rails, which can hold a module are placed in a level plane level. There is a mark on the rails such that it is possible to switch different modules while keeping their position identical. At both sides, there is a scope placed at the height of the centre of the module.
In order to establish a good reference line, first it is made sure that the rails are level. After this, the demo-module is used. This is a spare module without the rods, on which caps with small pinholes can be attached. This demo-module is placed upon the rails. Then, the scopes are made level using their internal spirit level. The height of the scopes is fixed by aiming the scopes at one pinhole. Using these steps we were able to make sure that both the reference line and the centre of this one pinhole is in one horizontal plane. By aiming both scopes at the centre of one pinhole and on the central vertical axis of the other

(a)

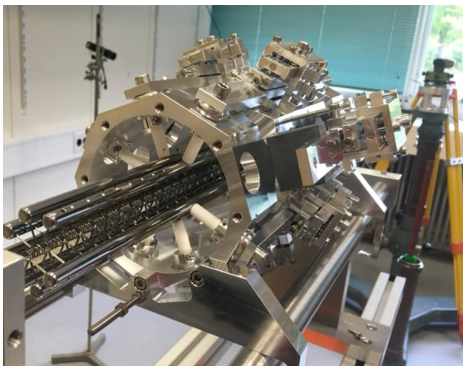

(b)

Figure 9: (a) Part of the setup used for transverse alignment of rods within the modules, showing a scope and a camera behind it
(b) The module on the rail with in the background the other scope and camera

it is ensured that the reference line of both scopes is also in same vertical plane. It is possible to place the rods one by one near the centre of the module. By placing a pointed rod inside the rings, the centre of the electrode can be determined. Adjustment screws on the module can be used to fine-tune the rod within the module, such that the centre of the electrode is the same as the centre of the scope. This process is repeated every time a new rod is placed near the centre. Cameras are place behind the scopes, their image is sent to a monitor. Allowing for real time feedback while using the adjustment screws, allowing for faster and more precise alignment.
After all the modules were aligned, the quality of the alignment was assessed. Via visual inspection it was concluded that the rods had a maximal error of 0.3 mm between each other. Although there is no specific value to compare this with, we are certain that this part of the alignment significantly improved. Using the cameras and a small brass pin which fitted through the first 4 rings it was determined how much drift there was from the reference line with respect to the central line traced out by the rings. This drift was typically of an order of 0.3 mm.

Longitudinal alignment
There are two methods of determining the distance between two consecutive rings. The first method uses a depth meter to determine the relative distance between the rods. Using adjustment screws on the module the distances are set properly within a margin of : 0.05 mm.
For some still unknown reason it appeared that the distance between the rings was not regular for certain modules after applying the above described procedure. For these few modules an alternative procedure was used. Using a camera in combination with a scope aimed the side of the module, it is possible to check

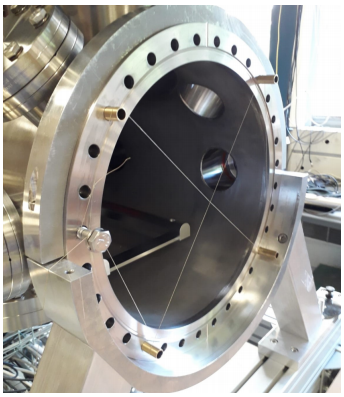

Figure 10: The crosshair created by spanning a thread used to determine the reference line. Figure from [10]

the distance between the rings visually. The obtained precision by this method is estimated to be 0.1 mm.

3.1.3 Aligning the rails

To align the rails the reference line is determined in the following way. By spanning a small thread at the outer flanges, as seen from figure 10, it is possible to determine the centre of the vacuum chamber. By aligning the scope on the cross at the back flange cross (The back end is where the cryogenic source will be placed), and using the internal water level of the scope it is possible to get a level reference line through the vacuumchamber. This line is a little under the cross-hair in the front, the deviation is about 0.5 mm
The rails are attached to the vacuumchamber via an adjustment system, the so-called 'hat'. By using the screws in this hat system it is possible to, lift the rails, to tilt them and to rotate them. During realignment, some of the hats from the previous generation have been upgraded, such that all hats can also shift in the transverse direction. By putting the demo module on the rails, it was possible to compare the middle of the rails with the reference line. A separate water level was used to ensure that the rails stayed level while lifting the rails. After the height and level were correct, the rails was shifted transversely until the pinhole and the reference line were well aligned while the demo module was in the middle of the rails. Then, the demo module was placed at the front of the rails and rotated until the crosshair was on the middle of the pinhole. These last two steps were iterated until a minimum error of 0.3 mm was reached. It is possible to use lock-in screws on the adjustment system to fix the rails at that certain position.

3.1.4 Mounting the modules on the rails

Before the modules were placed inside the vacuum chamber, it was checked which modules would match best as a pair. This had to do with the drift from the reference line introduced in section 3.1.2. Furthermore, the modules were treated with compressed air to minimise the amount of dust that would be brought into the vacuum chamber. The modules were put in the decelerator with the new electrical connections attached to them (see section 3.2).
The distance between 2 modules is determined by fitting a small metal block between the rods of two different modules. The thickness of this block is equal to the gap between the two rods of different modules. We estimate as small error of 0.2mm in the longitudinal direction when both modules are on the same rails. In the case that the distance had to be determined between two modules on different sets of rails we estimate to have an error of 0.4mm. This error is larger because it is physically harder to reach those places due to the structure of the vacuum chamber, which influenced the precision of the placement of the modules.
When placing the modules the quality of the alignment is checked using a small pin. Unfortunately, the misalignment became greater than the 0.3 mm with the demo module. The misalignment with the modules was about 0.6mm. A remarkable feature was that the error mostly increased in the vertical direction. This suggests that the lock-in screws do not completely fix the rails and that it is a little tilted in the vertical plane.

3.1.5 Overview of the errors in the alignment

Error in alignment between electrode and rod		
	Error (mm)	Error (mrad)
Bending of rod longitudinal direction	0.1	3
Bending of rod transverse direction	0.05	2
Electrode twist		35
Error in alignment between rods in a module		
	Error (mm)	Error (mrad)
Centre of the rods transverse plane	0.4	
Distance between the rods *using dept hmeter ** using scope	0.05* / 0.1**	
Deviation from the central reference line	0.3	
Error in alignment between modules		
	Error (mm) 2 modules 1 rail	Error (mm) 2 modules 2 rails
Distance between two modules	0.2	0.4
Error in the transverse plane	0.2	0.4
Deviation from central reference line	0.6 or 2mrad	0.6 or 2mrad

3.2 Electrical connections

During previous, experiments the voltage at which the decelerator was operated was in a range of 1 kV to 4.5 kV. For the eEDM experiment, a voltage of 10kV is required. This increase in voltage is however problematic for the electrical connection used up to this point as shown in figure 11a. The problem arises from the fact that this connector piece contains many sharp edges. When there is an high voltage on objects with sharp edges, you have a high electric field potential. This can lead to unwanted discharges and thereby short circuit.
In order to prevent these discharges, the electrical connection has been redesigned (see figure 11b). The new design does not contain any sharp edges. It consists out of a hollow copper cylinder closed at one side, with a small notch which fits around the rod and the electrodes. There is also a spring in the cylinder to ensure that there is good contact between the connector and the next rod. During the placements of the modules it is made sure that there is indeed an electrical connection between the modules.

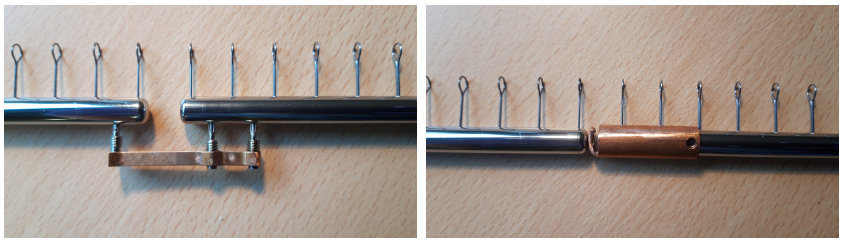

(a) (b)

Figure 11: (a) The old connection piece, which contains multiple sharp edges which poses a problem at high voltages. (b) the new connection piece, which is smooth and therefore capable of handling high voltages without having discharges

3.3 Conclusion

All the targets set for for the upgrade of the TWSD are met. The new reference line is at the centre of the flange at the back. The electrical connections are upgraded too, and are now able to handle a higher voltage appropriately. The alignment as a whole is also improved. As shown by the fact that it is possible to look through the decelerator. This was previously not possible due to a kink in the general line. Some of the rails adjustment systems have been upgraded such that they can shift. During this alignment stage we also gathered new and better data on the misalignment than before. This data can be used as input for simulations regarding the dependency of the efficiency of the TWSD on the alignment

4 Simulations of the misalignment

In order to quantify the dependency of the performance of the decelerator on the new alignment, it was decided to perform simulations. From the tables in section 3.1.5 it was suspected that there were two major sources of misalignment that would limit the efficiency.
One of these sources is the misalignment between the electrodes in the transverse plane within a module. Which can be seen as an imperfect overlap of the rings. The consequences of this on the efficiency of the decelerator is investigated in section 4.1.
In section 4.2, another effect of the misalignment on the efficiency is studied. These losses arise from the fact that the average positions of the electrodes not always follow the straight reference line in the vacuum chamber. Thus there are little kinks in the general path which the molecules take.

4.1 Misalignment between the electrodes in the transverse plane

During the realignment of the rods within a module an error of 0.4 mm in the transverse plane was introduced. This can be seen as not perfectly overlapping rings. In order to make a reasonable estimate of the loss of molecules due to this error some simulations have been performed. It is assumed that the molecules move fast through the single electrodes, and therefore the small irregularities in the electric field due to this misalignment are smeared out from the perspective of the molecules. Thus, the molecules do not experience a sudden change in their electric field potential. Under this assumption, the main loss mechanism is a molecule hitting an electrode. Furthermore, it is assumed that a trapped batch of molecules is uniformly distributed in the trapping volume. So if there is a trapped batch of molecules such a misaligned ring would in that case "shave off" a part of the molecular packet as is schematically shown in figure 12.

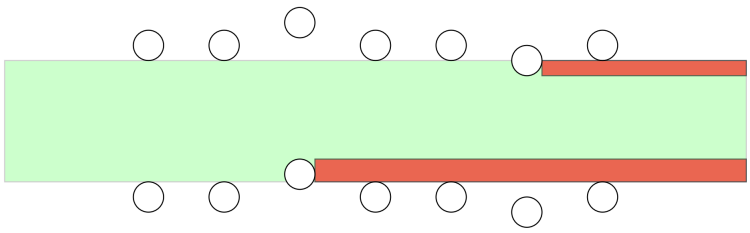

Figure 12: A schematic drawing of the cross section of the electrode-rings within a module. The red parts indicate the part of the molecular packet that would hit an electrode, due to misalignment, and would therefore be lost.

To obtain the fraction of molecules that would be kicked out by the deceler-

ator due to collisions with the rings a simulation has been made, see appendix B. In this simulation, points are randomly generated by an uniform distribution within an unit circle. Then a ring with the same radius but a different centre is generated. The place of the centre is normally generated such that it can resemble an error in the alignment. It is then checked whether the initially generated points also fit within this new ring. Once a point is not within a ring it is disregarded for the remainder of the loop within the simulation. Multiple rings can be generated within one loop. See also figure 13 for a visual representation. At the end of the simulation the ratio of initial points and the remaining points is is calculated.
In section 3.1.5 it was said that the maximum error found in this kind of misalignment was 0.4 mm. To make an accurate representation of this error inside the simulation it was made sure that on average 90 % of the randomly generated rings would fall inside this error bar by choosing the standard deviations in the simulations accordingly.
In a single simulation 8 rings were generated, because there are eight rods in a module. This simulation was performed with 5000 initial points and this simulation was repeated 500 times. Averaging over the acceptances gave an average acceptance of $\approx 76\%$.

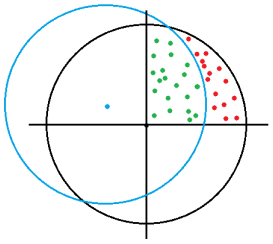

Figure 13: A schematic figure of the simulation. All dots are generated within the black unit circle but not all are within the second blue circle of which the centre, the blue dot, is picked from a normal distribution. So the green points are accepted and the red points are discarded. It is possible to do this for multiple rings in one simulation

4.1.1 Improving the simulation

One of the assumptions made by the model described above is that the density of molecules within a ring is constant. Which is not necessarily the case within the decelerator. In order to remove this assumption 3D molecular trajectory simulations are used(which will be described in more detail in 4.2.1). Using this simulation a more realistic distribution of points was obtained. This distribution is shown in figure 14. The distribution uses the x- and y-positions of molecules at two different timestamps to reduce the risk of systematic errors.

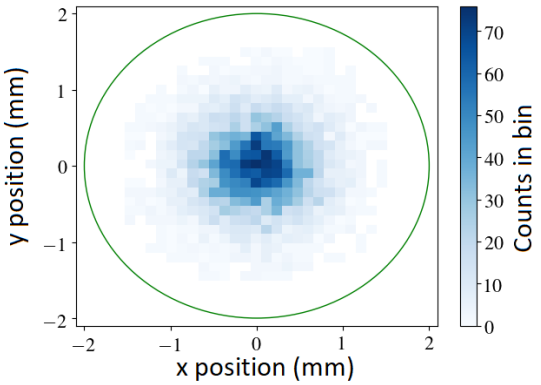

Figure 14: The combined distribution of 3000 molecules at two different timestamps, One timestamp was made at 10 ms and another at 15 ms.The green circle indicates the inner edge of the electrode. the density in the middle of the electrode is significantly higher than at the sides. Indicating that small errors in ring overlap will probably not affect the efficiency much.

Repeating the simulation but replacing the random generated points by these realistic points gave a far higher acceptance. The results of the simulation are shown in figure 15 for different errors. From the graph it becomes clear that small errors, within 1.0 mm, will not lead to significant losses. Our error of 0.4 mm fits very well within these restraints, thus it seems that the imperfect overlap does not lead to a severe decrease in efficiency.
It is important to note that some assumptions probably will not hold when the error becomes large. For example the assumption that the disturbance in the electric field will not affect the molecular trajectory will become less valid as the error increases.

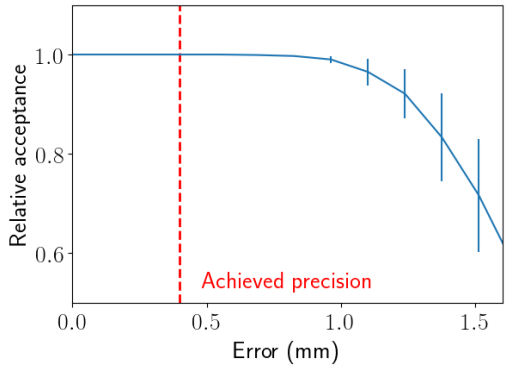

Figure 15: The relation between the efficiency and the error of the rings in the transverse direction. Curve is only given for explanatory purposes. The error is marked by the red bar and it becomes clear that this precision is well within the threshold of being not a source of a significant error.

4.2 Rotation between modules

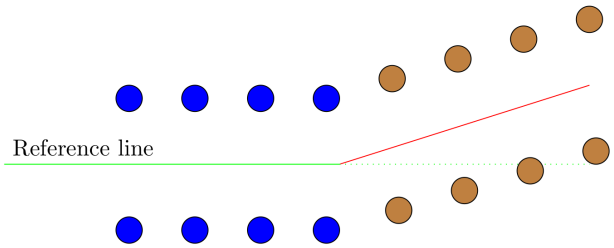

Figure 16: A schematic drawing of the cross section of the electrode-rings between two modules (indicated by blue and brown). There is a kink with angle ϕ between the two modules. A schematic drawing of the of a kink ϕ between two modules

When realigning the modules on the rails, it was found that there were some significant deviations from the reference line, (see figure 16). The error is 2 mrad and even though this is similar to before the disassembly, it is still worth investigating, in order to quantify the performance of the TWSD. There are multiple possible contributions to these deviations. For example there is already a deviation from the reference line from the way that the rods are not perfectly aligned within the modules themselves. Another suspected source of a deviation is some movement of the rails itself. From the information we have of the alignment, it can be induced that a certain angle between the rails and the reference line in the vertical plane is introduced. In order to estimate the effect

on the performance of the TWSD due to this misalignment, simulations have been used. First, the simulation are introduced and then some additions are applied in an attempt to mimic the misalignment.

4.2.1 Structure of the molecular trajectory simulation

The NL-eEDM group has developed a simulation to simulate the trajectory of the molecules throughout several parts of the setup, which is described in detail by Muller [11]. The goal of this simulation is to model the motion of molecules from a molecular source through the TWSD and the free flight until detection. This allows us to compare experimental results with some theoretical framework. It is also a gateway to more knowledge on the behaviour of the molecular beam inside the decelerator, for which we do not have experimental data. The simulation can be separated into three parts closely resembling the physical reality.
The simulation starts with generating molecules using pseudo-random number generators that generate a random point in 6 dimensional phase space. This can be done in such a way that the resulting distribution resembles one that is created by the source used. The molecules then have a distance of free flight after which they enter the decelerator.
Simulating the motion inside the decelerator is the most complex part of the simulation. First, the magnitude of the electric field inside the decelerator is simulated. This is done by first obtaining values of the electric field at different points via COMSOL and then interpolating those values. Once this electric potential is determined, it is possible to connect its gradient to a force using the Stark curves, as discussed in section 2.1. Since now there is a force, the resulting equation of motion of the molecules can be solved by numerical integration. The integration method used in the whole simulation including the free flight is a fifth order Runge-Kutta method.
Once the molecules exit the decelerator their free flight motion is simulated and the molecules can cross the LIF detection, which saves the timestamp of the molecule passing that longitudinal position.
In order to quantify the performance of the decelerator we use the term acceptance. Acceptance is the ratio of the molecules that are trapped throughout the decelerator w.r.t. the total amount of molecules generated. We call a molecule successfully trapped in the central trap when it is within a radius of 2 mm in the transverse direction of the central line of the decelerator and within 3 mm behind and 3 mm in front of the central trap.

4.2.2 Modelling the effect of the angle

In order to model the rotation we make a few assumptions. First we assume that the end of one module always perfectly overlaps with the start of the consecutive module. It is thus assumed that the deviation from the reference line is entirely caused by the angle between two modules. Secondly, we assume that the effect on the electric field inside the decelerator is similar apart from the fact that it

is rotated, so edge effects are neglected.
With these assumptions we can model this angle as a rotation of the velocity vector of the molecule as shown in figure 17. So the transformations are $V_{\text{trans}} = V\sin(\theta) \rightarrow V'_{\text{trans}} = V\sin(\theta+\phi)$ and $V_{\text{long}} = V\cos(\theta) \rightarrow V'_{\text{long}} = V\cos(\theta+\phi)$.

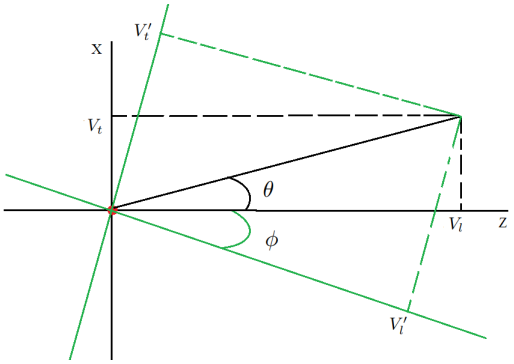

Figure 17: A figure on how a molecule going from one module to another with an angle ϕ results in a rotation in the coordinate system of that molecule. θ is the angle between the transverse and longitudinal component of the velocity vector before the transformation. So in the initial frame, $V_{\text{long}} = V\cos(\theta)$ and $V_{\text{trans}} = V\sin(\theta)$. While in the new frame : $V'_{\text{long}} = V\cos(\theta+\phi)$ and $V'_{\text{trans}} = V\sin(\theta+\phi)$

We know from the separatrix plots that the transverse velocity of accepted molecules is a few m/s and thus much smaller than the longitudinal velocities varying between 200 m/s and 30 m/s. Therefore, the angle between the longitudinal and the transverse velocity ,θ, is small. The angle ϕ that we achieved was maximally 2 mrad, which is also small. Thus it is justified to use the small angle approximation: $V_{\text{trans}} = V\cdot(\theta)$ and $V'_{\text{trans}} = V\cdot(\theta+\phi)$. So moving from the initial frame to the next frame essentially is just a a kick in the transverse velocity of $V\cdot\phi$, where $V \approx V_{\text{long}}$. It is important to note that a leak from one longitudinal velocity to transverse velocity is far more impactful with respect to possible losses than the other way around. By a small angle approximation it can be seen that the latter is only a second order change. So the dominant loss channel would be a kick out of the transverse acceptance.
To see how such a velocity kick influences the efficiency of the decelerator we take a look at the separatrix. A velocity kick would mean a vertical shift for all the molecules in the separatrix, causing some to fall outside of the separatrix, as is shown in 18. Thus these molecules would no longer be trapped.

4.2.3 Implementing the model

Modifying the numerical integrator of the simulation
In order to implement these velocity kicks the numerical integrator of the simulation was updated. Every 500 mm from the first module it performed the

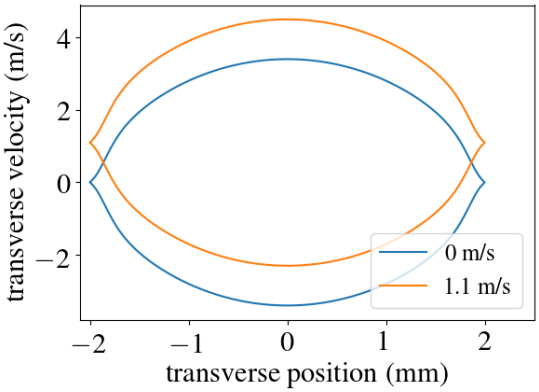

Figure 18: A positive velocity kick would shift the separatrix. So the common area of the seperatix is smaller. A 1.1 m/s velocity kick corresponds to a 6 mrad rotation at a velocity of 200 m/s

transformations given in 4.2.2. The angle ϕ can be varied. The situation which most closely resembled the rotations in the modules, is the one in which the angle ϕ was applied alternating between positive and negative, resulting in a zigzag pattern of the modules.
Data was obtained for different angles and guiding velocities. The initial distribution that was used was representative for a supersonic source described by Zapara [8]. From this data, it was concluded that the velocity kicks indeed followed the small angle approximation. It was also found that indeed the losses in the longitudinal direction were negligible.
From the obtained data an efficiency of 90 % was suggested for guiding at 200 m/s at our error of 2 mrad. By comparing the efficiencies of the other measured guiding velocities we were able to check the validity of this method. From the model it was known that at higher guiding velocities the velocity kick would be be greater. This has also been verified within the simulation. However, one would expect that the efficiency would remain somewhat constant for similar velocity kicks independent of the guiding velocity. This was found to be not the case. Besides that it was hard to reproduce the data for it was very sensitive to small changes. Therefore it was chosen to not continue with this particular investigation.

Using the separatrix
By assuming an uniform distribution of the molecules inside the transverse separatrix these velocity kicks can be connected to an efficiency via a shift of the separatrix. For a rotation of 2 mrad at 200 m/s guiding a velocity kick of 0.4 m/s is obtained. The reduced area of the separatrix is calculated. It is found that such a velocity kick would limit the efficiency to approximately

95 %. This is however only be valid for one velocity kick. In the case of a zigzag pattern the molecules would be kicked down in velocity again. However the molecules within the separatrix would have evolved over time and would be able to redistribute themselves within this (new) separatrix. In the worst case scenario, the molecules are again uniformly distributed across the separatrix by the time they get a new velocity kick. Which would mean an efficiency of 66 %. In the best case scenario, where there is no redistribution in the separatrix, the efficiency would stay at 95 %.

4.3 Conclusion

Two major sources of error have been investigated. It is found that our achieved accuracy for the transverse alignment of the electrodes is good enough that it will not reduce the efficiency of the decelerator.
Rotation between the modules does however introduce a significant loss of molecules. The data obtained from the 3D simulations was assessed to be not reliable. From an analysis of the separatrix in combination with the concept of a velocity kick, we are able to give a limit on the reduced efficiency of 66% - 95%.
But one should keep in mind that the during all of the reassembly the alignment the precision of the alignment, on all fronts, has improved or at least stayed on the same level w.r.t. the previous alignment. And therefore the decelerator is still expected to work efficiently.

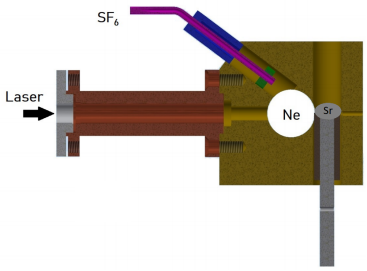

Figure 19: A schematic figure of the cryogenic source

5 Loading molecules from a cryogenic source into the decelerator

In this chapter it is shown that the decelerator performs after its reconstruction and connection with the cryogenic source. It would be useful to compare the data obtained from the newly realigned TWSD, with data of the decelerator before it was disassembled. However, the TWSD is now connected to a cryogenic source, this used to be a supersonic source. In this chapter the effects that this new source has on the eventual time of flight (ToF) profile is discussed, as compared to the supersonic source to see whether the both could be compared.

5.1 The phase space distribution from the cryogenic source

5.1.1 The cryogenic source

The goal of the cryogenic source is to create as many slow SrF molecules as possible, generally this is a velocity of 200 m/s. Which is lower than for molecules originating from a supersonic source which have a typical velocity of 350 m/s. For a thorough description of our cryogenic source see the master thesis of Hof [12]. Here only a general and brief summary of a cryogenic source is given.
The cryogenic source uses buffer gas cooling to cool molecules [13]. This works in the following way. An ongoing stream of a gas mixture consisting out of SF_6 and chemically inert Ne is cooled down in several cooling stages. It eventually enters the main cell at a temperature of typically 16 - 25 K. In that same cell there is a ablation target consisting out of Sr metal. With a frequency of 10 Hz this target is ablated by a Nd:YAG laser with a short burst of typically 20 mJ. These high energies cause some of the Sr metal to evaporate. This hot Sr can react with the SF_6 in the mixture forming SrF with a high temperature. These diatomic molecules will thermalize through approximately 50 elastic collisions with the Ne to this low 20 K temperature. Finally, the molecules leave the cell through the cell exit which has a diameter of 4.5 mm and which is 9 mm further down from the ablation spot.

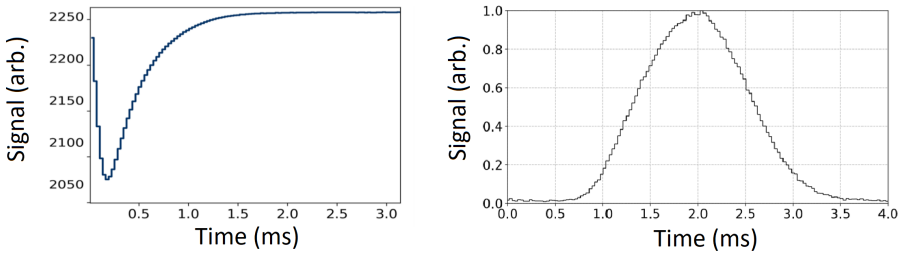

(a) (b)

Figure 20: (a) A typical absorption signal taken from the absorption setup (b) A ToF measurement of the LIF setup

5.1.2 The setup of the cryogenic source measurements

In order to characterise the distribution of molecules that the cryogenic source supplies, two parallel measurements are performed. Namely a laser absorption measurement and a LIF measurement. The absorption measurement takes place 5 mm from the cell exit and the LIF is at 30 cm from the cell exit.
The laser absorption setup works as follows. The laser light which is resonant with the SrF $X^2\Sigma^+(v = 0, N = 0) \rightarrow A^2\Pi_{1/2}(v' = 0, J = 1/2)$ transition at 663 nm, is aimed perpendicular to the beam. Some of this light is absorbed and emitted into a random direction through spontaneous emission and is thus very unlikely to reach the photodiode further down the setup. The photodiode therefore senses a dip in the intensity of the laser light. This dip is proportional to the density of molecules. Resulting in graphs like in figure 20a.
The LIF setup works at the same transition as the absorption setup. The laser transverses the molecular beam from a perpendicular direction once. And is then reflected back and transverses the molecular packet once again. When the molecules absorb a photon it can spontaneously emit a photon. This spontaneously emitted photon is emitted in a random direction. Normal to the laser beam and the molecular beam there is a construction used for collecting these spontaneous emitted photons and focusing them into a photo multiplier tube (PMT). The PMT can register individual photons and by making a timestamp when a photon arrives allows for making ToF figures like figure 20b.

5.1.3 Analysis

Because the absorption measurement is performed only 5 mm from the cell exit the distribution of the molecules in the packet did had very limited time to evolve according to its velocity distribution. Thus it is reasonable to assume that the absorption measurement closely resembles the positional distribution. So the graph in figure 20a shows that a typical molecular packet, originating from a cryogenic source, has a FWHM width of around 0.3 ms. The packet travels with a typical velocity of 200 m/s, so the FWHM of the packet is $\approx$

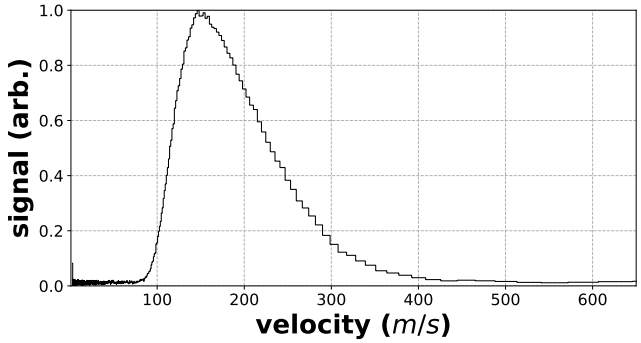

Figure 21: The resulting velocity spread by transforming the time axis of figure 20b to a velocity axis, assuming a point source.

60 mm.
The LIF measurement is further down the setup and allows for a characterisation of the longitudinal velocity distribution of the molecular packet. In contrast to the absorption measurement, here the molecular packet has had more time to evolve according to its velocity distribution. So features that exist in the ToF profile are also present in the velocity distribution. Assuming a point source a velocity distribution given by figure 21 can be approximated. This distribution has a FWHM of $\approx$ 100 m/s. The fact that this gives a skewed Gaussian, is likely to be a result of the point source assumption not being entirely valid.
The initial width and the wide velocity spread are both larger with respect to the previous source, the supersonic source. Which had a positional width of around 10 mm and a FWHM value of approximately 15 m/s for the longitudinal velocity distribution.

5.2 A cryogenic source coupled to the decelerator

Here it is discussed how the decelerator handles the broad molecular packets delivered by the cryogenic source, both in positional space and velocity space. It is also discussed how this affects an eventual ToF profile taken after the decelerator.

5.2.1 filling multiple traps

In section 2.2 the principles of the TWSD were explained and it was shown how a molecule can be trapped in electrical potential traps. In the TWSD there are multiple traps with a periodicity of 6 mm, see figure 6. Thus, if the molecular packet is broader than 6 mm, then molecules from the same packet get captured in different traps. In the case of the previously characterised cryogenic source, around 10 to 30 traps are expected to by filled.
In order clarify these multiple traps being filled, figure 22 shows a sheet in phase space and how a molecular packet evolves within in. The molecules start from

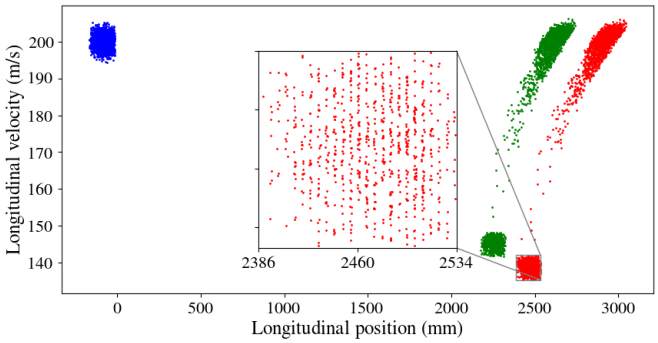

Figure 22: The evolution of the phase space distribution at a deceleration of 4.2 km/s^2. The blue dots indicate the accepted molecules 0.5 ms after they were generated from a source, the green and red dots are timestamps taken at 13.5 ms ms and 15 ms respectively. The chosen longitudinal velocity spread is not representative for the cryogenic source.

a distribution that has a significant width in the longitudinal position indicated by the blue dots. Then some of the molecules are trapped by the decelerator and subsequently tried to be slowed down. However, the majority of the particles is not captured and is only transversely confined. Those particles keep the same velocity and that part of the packet starts to rotate in this 2D phase space, increasing their correlation between velocity and position. The diluted region between these two regimes are molecules who were slowed down initially but the trajectory in the trap was not stable and consequently they got stuck in the middle.
In the inset of figure 22 it is shown that in the packet of the slowed down molecules there is also a substructure. This periodic structure of 6 mm is caused by the fact that multiple traps are being filled. The broader the the position in the longitudinal direction the more different traps will be filled. This can be clearly seen from the ToF plots in figure 23. The periodicity of 30 μs shown in these ToF profiles corresponds to the periodicity of 6 mm at a guiding velocity of 200 m/s. Thus once multiple traps have been filled the ratio between these traps gives information about the distribution as it entered the decelerator. So from the structure between the peaks in a ToF profile we can induce a longitudinal position distribution.

5.2.2 Molecules outside the velocity acceptance

As explained, the decelerator has a typical longitudinal velocity acceptance of $\pm$ 5 m/s for SrF molecules. This means that in the case of the cryogenic source that roughly 95 % of the molecules will not be within this acceptance. For, as was shown before, the typical velocity spread of our packet is of the order of 100 m/s.

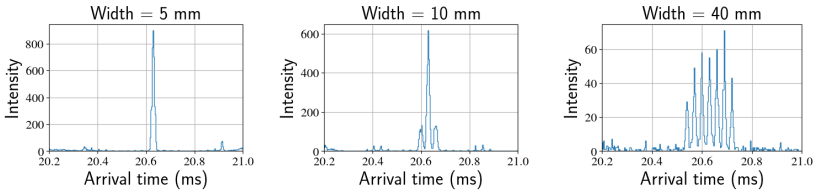

(a) (b) (c)

Figure 23: Some typical ToF profiles for different initial longitudinal widths (a) a width of 5 mm (b) a width of 10 mm (c) a width of 40 mm. A wider initial distribution leads to more traps being filled.

Even though these molecules are not trapped, they influence ToF profile. Since They still experience the transverse trapping potential and thus do not suffer large losses in the transverse direction. Furthermore, even though they are not trapped, their velocities will be slightly bunched by the traps, this will be visible as a modulation in the signal with the same periodicity of the traps.

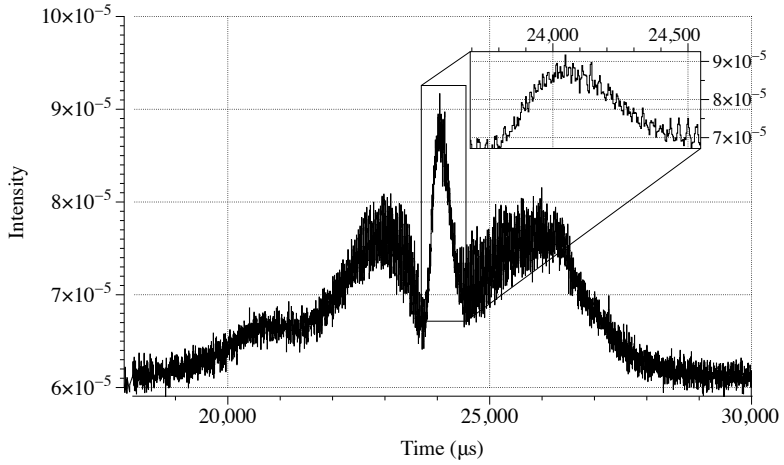

Figure 24: A ToF profile of the reassembled 4.0 m TWSD, guiding at 190 m/s with a voltage of 3.0 kV

5.3 The experimental results

The cryogenic source is coupled to the TWSD. In order to characterise the the performance of the cryogenic source in combination with the newly aligned decelerator a LIF detection setup is put 120 mm after the exit of the decelerator. This LIF setup is similar to the one introduced in section 5.1.2. In figure 24 one of the resulting ToF profiles is shown.

From the inset it becomes clear that multiple peaks have been filled, as was expected from such a wide molecular packet. It seems that approximately 25 traps are filled.
Besides that there are also molecules outside the longitudinal velocity spread. Those molecules show a kind of modulation at 21 ms. That is as of now not yet fully understood. Also the velocity width of the molecules outside the velocity acceptance seems to be too small for the 100 m/s FWHM value given in section 5.1.3. A more reasonable value seems to be 50 m/s. One reason for this difference comes from the fact that the high voltage amplifiers driving the decelerator are on for a limited amount of time per molecular packet. Thus for slow molecules the transverse trapping stops earlier in the experiment and are therefore likely to be lost, effectively narrowing the velocity distribution on the slow side side. Another reason for this discrepancy is that the point source approximation used to extract this 100 m/s value is not valid, for the molecular packet is too wide for this assumption. Thus, a FWHM value of 50 m/s fits the velocity distribution better.
In figure 25 a ToF profile of a 2.0 m TWSD in combination with a supersonic source is given. This ToF profile is different from the newly obtained ToF profiles in multiple facets. The small positional width allows for only 1 to 3 filled traps. The small longitudinal velocity distribution is reflected in the low amount of molecules besides the trapped molecules.

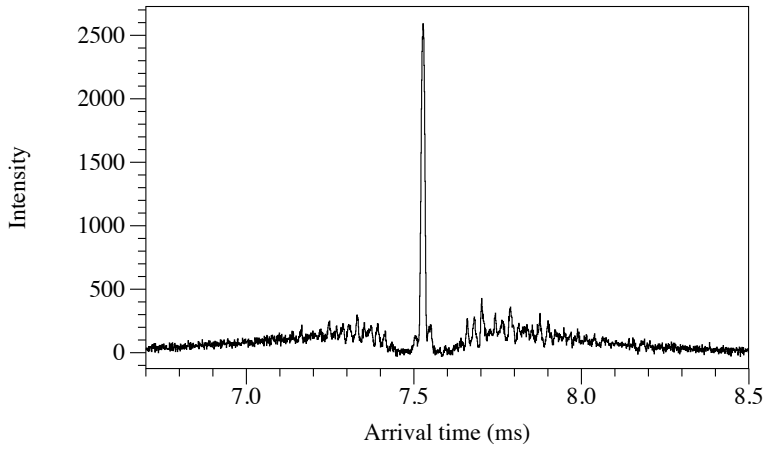

Figure 25: A ToF profile of the 2.0 m TWSD in combination with the supersonic source at a guiding velocity of 350 m/s

5.4 Conclusion

The phase space distribution that the cryogenic source delivers differs vastly from the what the super sonic source delivers. The cryogenic source supplies a

initial distribution of molecules that has a spatial FWHM $\approx$ 60 mm, in contrast to the supersonic source which supplies packets with a width of 5 mm. This large width causes multiple of the 6 mm periodic traps to be filled.
The molecules from a cryogenic source have a velocity distribution that can be approximated to be a Gaussian with a FWHM of 50 m/s. Which is wide as compared to the supersonic source which has a FWHM of 20 m/s. This wider distribution means that there are many molecules that are out of the longitudinal velocity acceptance, and thus will only be transversely guided. Causing a lot of signal outside the trapped region.
All the discussed features are observed in the first experimental results of the TWSD in combination with the cryogenic source. Except from the modulation in the signal. Due to the different sources used, it is not possible to compare these new results with the results from the TWSD in combination with the supersonic source to extract some information regarding the performance of the decelerator.

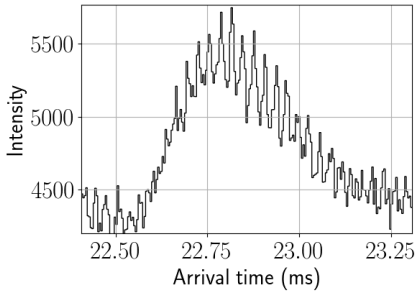

Figure 26: A zoom-in on the peak structure of an experimentally obtained ToF profile

6 Comparison of simulations with experimental results

In this section we would like to use molecular trajectory simulations to obtain information on the performance of the decelerator. The experimental ToF profiles are analysed such that these results can be reproduced via the molecular trajectory simulations introduced in section 4.2.1. First 1D simulations are used and finally the full 3D trajectory simulations are used. Once a ToF profile is successfully recreated within the simulation, the performance of the simulation is benchmarked. This is done by changing the parameters of the simulation and comparing this new ToF profile with the experimental results of the same parameters. If that is successful then the simulation will be used to extrapolate for not yet measured voltages and deceleration strengths.

6.1 Reconstructing the ToF profile in 1D

6.1.1 The shape of the peak

The simulation should be able to handle full 3D trajectory simulations. However, it was found that when large longitudinal velocity spreads were used, the 3D simulation showed a heavy modulation in the ToF profile. This modulation is not yet completely understood. Therefore the simulation is first reduced to a 1D simulation which does not show this modulation. This is achieved by setting all transverse components of the molecules to zero. Meaning that the generated molecules do not contain any transverse velocity component, nor do they start out with a transverse offset from the central axis. The simulation will be opened to 3D in section 6.3 .
In order to get a better understanding of the initial distribution from the cryogenic source and to check whether the simulation behaves properly, it is important to recreate the experimental signal using the simulation. There are a few characteristics that need to be reconstructed.

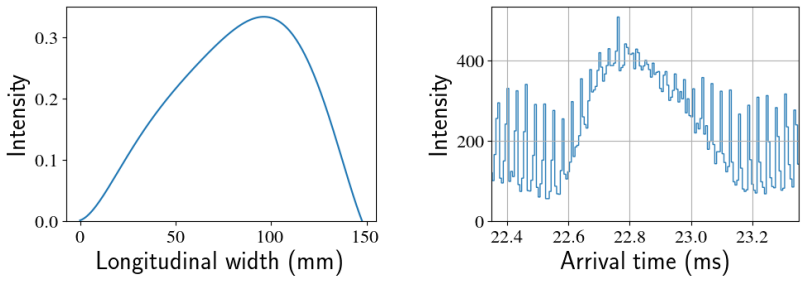

(a) (b)

Figure 27: (a) The longitudinal positional distribution obtained by the procedure described in section 6.1.1. (b) The resulting ToF profile from the simulation using this distribution. The characteristics of the experimental results of figure 26 are still present

One of these characteristics is the shape of the ToF profile caused by the molecules which were not within the longitudinal velocity acceptance. This part of the signal would have a similar shape as the velocity distribution. However the experimental results show a kind of modulation which is not yet understood. It is suggested that this modulation is connected to the modulation seen in the 3D simulations. Therefore, the modulation is neglected for the 1D simulation and the velocity distribution is approximated to be a Gaussian. We can justify this assumption as this would be the measured velocity distribution of only the cryogenic source before the coupling, shown in figure 21. By trial and error it was found that a FWHM of 15 % of the mean longitudinal velocity fitted reasonably well.
The mean velocity of the beam is dependent on several parameters of the cryogenic source: the Ne flow through the cell; the power of the ablation laser and the temperature of the cell. But generally the mean initial velocities during the experiments treated in this thesis are within 190 m/s and 210 m/s.
In figure 26 it is shown that although multiple traps are filled, not all the traps are filled with the same amount of molecules. As discussed in section 5.2.1, the way these traps are filled is proportional to the positional distribution at the moment of entering the decelerator.
The analysis of these multiple filled traps is done in several steps. First the ToF data around the peak is extracted. These timestamps are then bunched into bins. The binsize is chosen in the order of the width of the traps such that the substructure of the trap is averaged out. Subsequently, the background is subtracted from the data set by setting the lowest bin to zero. Then a 6th order polynomial is fitted through these bins. This line is than normalised and reversed. The result of this procedure is the longitudinal distribution shown in figure 27a.
Using this distribution to generate molecules in the simulation resulted in ToF

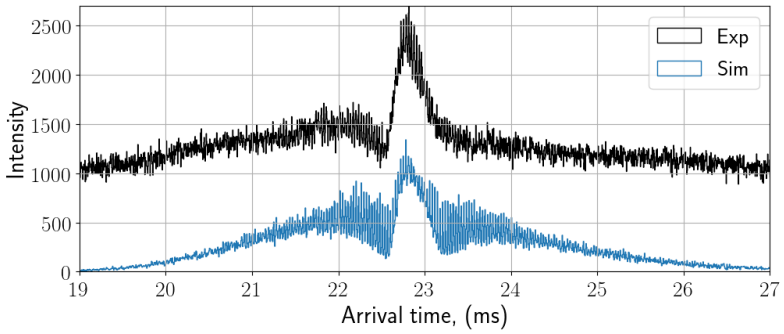

Figure 28: The experimental data which was analysed such that it could be recreated by the simulation and the the final simulated result

profile of the captured molecules shown in graph 27b. The fact that the shapes are similar corroborates the hypothesis that the structure of the peaks between themselves does indeed give information regarding the longitudinal position distribution.

6.1.2 The parameters of the simulated graph

In table below there is a summary of the parameters used in the simulation to generate the molecules that recreate the experimental signal of the 200 m/s guiding at 3.0 kV, as shown in figure 28. The timing of the simulation was 0.1 ms slower and was shifted artificially after the gathering of the data.

Input parameters for the initial distribution, 1D simulation	
Longitudinal positional dist.	Custom (see figure 27a)
Longitudinal velocity dist.	Gaussian, FWHM = 15% of mean velocity
Mean velocity	190 m/s - 210 m/s

6.2 Extrapolating the 1D simulation

6.2.1 Different voltages

By only varying the voltages of the simulation and comparing the resulting ToF profiles with the experimentally obtained ToF profiles it is possible to benchmark the simulation. The simulated results for different voltages are shown in figure 29

The results of the simulation suggest that the only effect of using different voltages is the amount of molecules that is trapped within the guiding potentials. There seems to be an optimum at 4 kV for the amount of captured molecules. The shape of the molecules outside the velocity acceptance is not influenced

significantly.
When simulated data is compared to the experimental data , shown in figure 30, multiple differences can be found. Most notable is the difference that occurs at 2 kV. For at 2 kV the experimental result completely vanishes while in the simulation there are no irregularities. It is however important to realise that the 1D simulation has no loss mechanism and thus will never be able to reproduce such a null signal. Another difference, is that the experiment seems to show a maximal amount of trapped molecules at 3 kV, compared to the simulation that shows an optimum at 4 kV.
So these differences suggest that extrapolating the simulation into other voltages will not properly represent the physical reality.

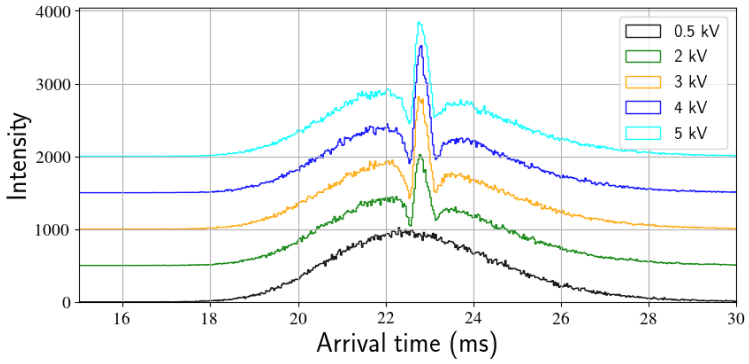

Figure 29: The recreated 1D ToF profiles using the simulation for different voltages, at a guiding velocity of 210 m/s

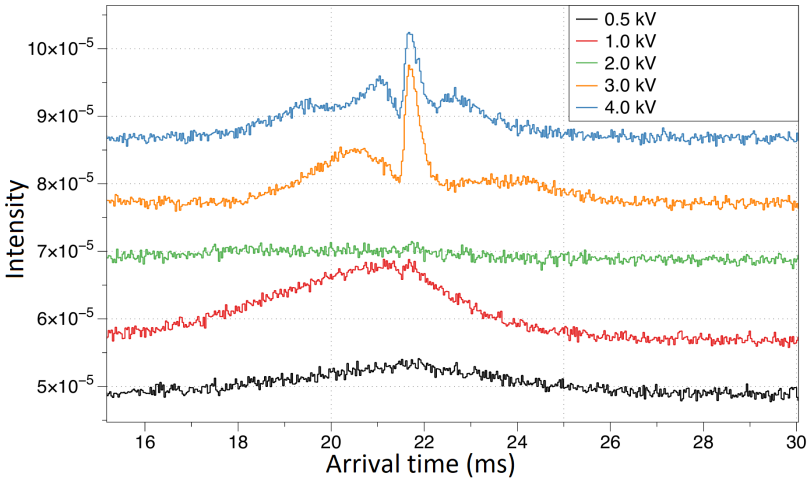

Figure 30: The experimentally obtained ToF profiles for different voltages at a 210 m/s guiding velocity

6.2.2 Different deceleration strengths

The simulation is used to simulate different deceleration strengths. The results of the simulation shown in figure 31 are compared to the experimentally obtained results shown in figure32.
Apart from the modulation in the experimental signal, both signals show the same deceleration features. It is noteworthy that the final arrival times of the packets are different, the experimental packet arrive about 0.3 ms earlier for the strongest decelerations. The simulation does agree with a separate back of the envelope calculation of the arrival time. Thus, this discrepancy is likely to be caused by some experimental detail.
The simulation can also be used to predict losses of trapped molecules due to deceleration w.r.t. guiding. And even though this is a 1D simulation these numbers are still relevant because, the transverse potential should be independent of deceleration strength, and the relative efficiencies in the 1D simulation should therefore be similar to the 3D result. From the simulation we get the following ratios:

Efficiency of deceleration from simulations	
170 m/s guiding	100%
170 m/s -> 130 m/s	88%
170 m/s -> 110 m/s	73%
170 m/s -> 90 m/s	64%

Comparing these ratios with the ratios obtained from the experiment would allow for making a statement about the performance of the decelerator. However it is unclear how to separate the decelerated packet from the background consisting out of molecules that are not within the velocity acceptance. This is because the background is not constant for the different measurements, probably due to shifting experimental parameters. Therefore, it was decided not to extract these values from the experimental results.

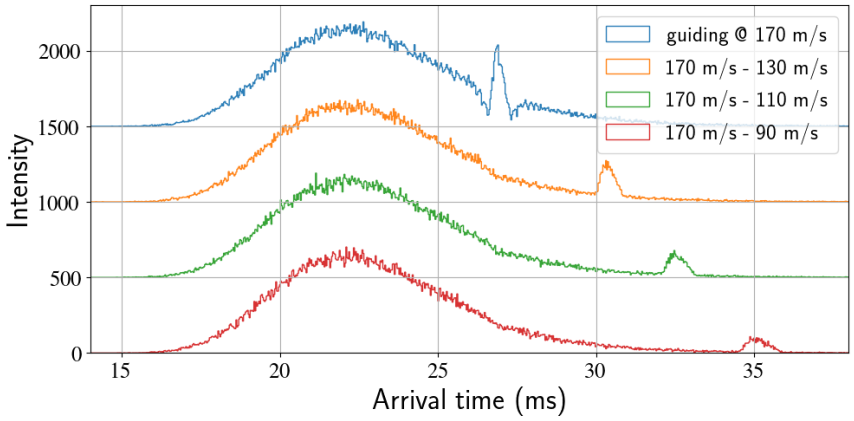

Figure 31: The recreated 1D ToF profiles using the simulation for different deceleration strengths, at a voltage of 3 kV

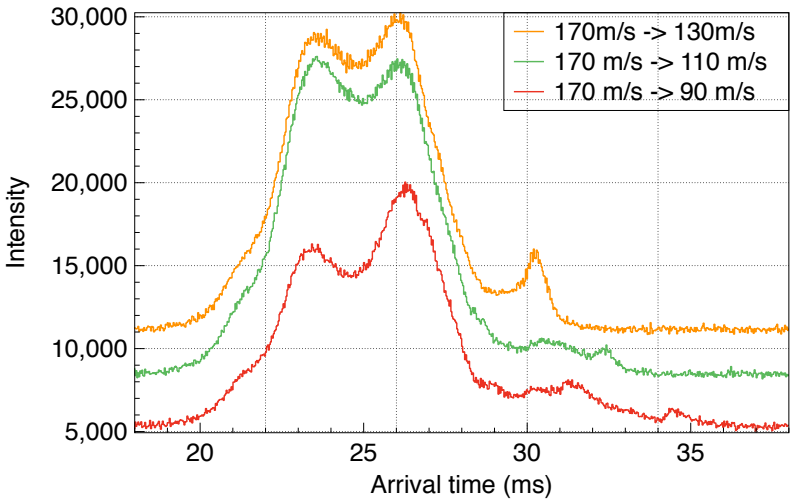

Figure 32: The experimentally obtained ToF profiles for different deceleration strengths at 3 kV

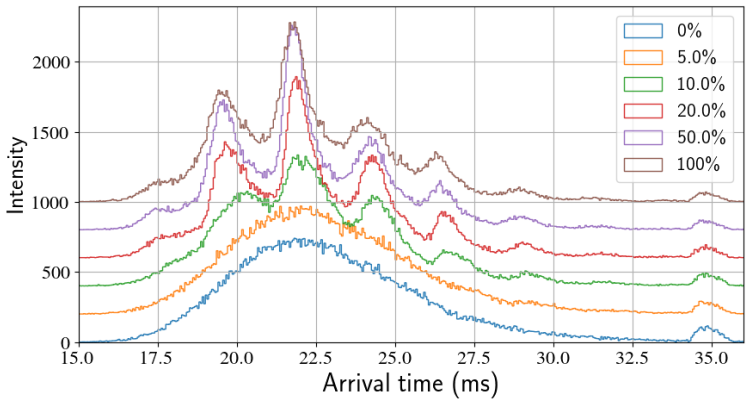

Figure 33: A ToF profile at 3 kV decelerating from 170 m/s to 90 m/s, The percentages indicate the amount of transverse components that are allowed. The more transverse components the heavier the modulation becomes.

6.3 Opening the simulation up to 3D

For a better understanding of the modulation of the experimental results the 1D simulation is opened up to the 3D simulation by gradually allowing transverse components. The transverse components of the molecular packet are limited in the following way. The radial offset of the molecular packet is limited by the geometry of the cell exit of the cryogenic source. This is a circular orifice with a diameter of 4.5 mm. The distribution used to generate this component is a truncated Gaussian with a standard deviation of 1.0 mm and it is truncated at the edges of the orifice.
The transverse velocity spread of the packet is of the same order as the forward velocity spread [12], so $\approx$ 50 m/s. This distribution is most likely similar to a Gaussian. However, the distance between the source its cell exit and the decelerator is 369 mm. The rings of the decelerator are only 4.0 mm in diameter. At a velocity of 200 m/s this means that most of the molecules will miss the rings. Only the part going from -2 m/s to +2 m/s has to be simulated. This small part of the Gaussian is approximated to be an uniform distribution.
By introducing a parameter in all these transverse components and varying this from 0 to 100 % the simulation can be gradually opened to transverse losses. The result is shown in figure 33. The simulation shows a modulation that increases as the transverse components are gradually turned up. The modulation eventually becomes more severe than seen in the experiment. And even though the modulation does not perfectly fit with the modulation in the experimental signal the presence of this kind of modulation within the simulation suggest that there could be a connection. Therefore, it is worth to investigate this modulation in the signal in more detail.

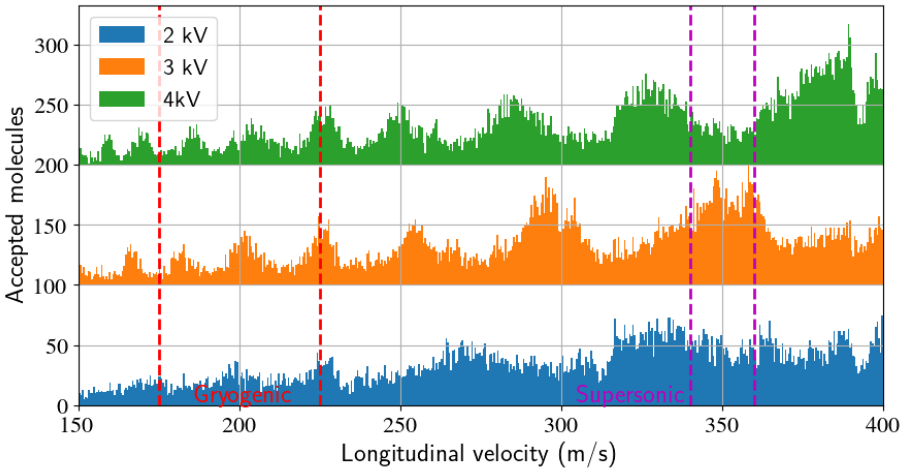

Figure 34: The amount of molecules that were within the acceptance of the decelerator plotted against the longitudinal velocity, at 3 kV. The molecules have been uniformly generated across the longitudinal velocity. So the dips in the intensity indicate a reduced ability to transversely guide the molecules. The demarcated regions represent the operating velocities for the different sources. The general downward trend of the accepted molecules form higher to lower velocities is due to the fact that there is a free flight of 369 mm before entering the decelerator

6.4 Investigating the loss mechanism in the 3D simulation

The modulation within the 3D simulation is not well understood. In this section it is investigated what the dependencies on this modulation are and what how these molecules get lost.

6.4.1 A reduced transverse confinement

To investigate the modulation in the simulated 3D ToF profile, a special initial distribution is used. Molecules are generated uniformly in a longitudinal velocity width of 250 m/s. Then it is checked whether these molecules are accepted by the decelerator. Of all these accepted molecules their initial longitudinal velocities are plotted in a histogram as shown in figure 34.
In the plot above a guiding velocity is set at 420 m/s. Such that all simulated molecules fall outside the velocity acceptance. Thus, no molecules are trapped, they are only transversely guided. In order to test for systematics this guiding velocity was taken in multiple values. This did not influence the acceptance at different longitudinal velocities.
Although the same simulation has been used for previous simulations in 3D, for the supersonic source, it did not show any modulation before. The reason

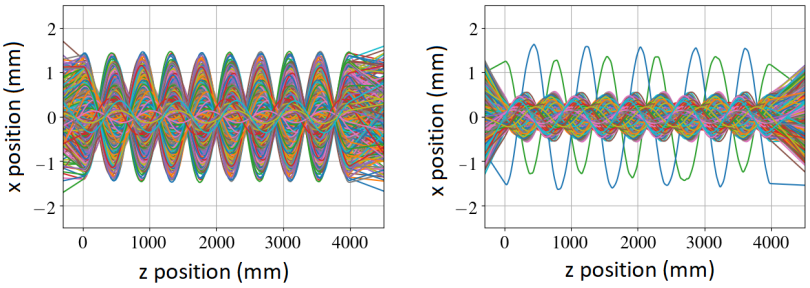

(a) (b)

Figure 35: The trajectories of 500 molecules outside the velocity acceptance of the 200 m/s guiding potential at 3kV (a) Here the molecules molecules are generated at a velocity of 234 m/s e.g. here the acceptance is high (see figure 34) (b) In this plot the molecules have a velocity of 223 m/s which is region where the acceptance is low.

for that is that the velocity width of the supersonic source is smaller than the velocity width of the cryogenic source. This means that only a small region in longitudinal velocity space is used. And the differences between the acceptances is small within that region.

6.4.2 The trajectories for different longitudinal velocities

To get more details regarding the different regions of low and high acceptance, the trajectories of the molecules in these different regions are plotted. The plots are shown in figure 35.
From the plots it can be induced that for molecules in a high acceptance region, a significant amount of the the molecules is allowed to deviate quite a bit from the principal axis during the guiding. Whereas at the low acceptance region the trajectories are confined to a small area around the principal axis. This point is restated in figure 36.
It was also found that in neighbouring high acceptance regions the number of nodes in the trajectory differed by one. Suggesting that this effect has something to do with resonances.

6.5 Conclusion

Using analysis of the data we were able to recreate the ToF profile for a 3 kV, 190 m/s guiding signal in a 1D simulation, as is shown in figure 28, except for the structure of the molecules outside the velocity acceptance. The extrapolation of this simulation across different voltages does not agree with the experimental result. Where the simulation shows a very regular pattern compared to an erratic pattern in the experiment. Which could have been caused by not in-

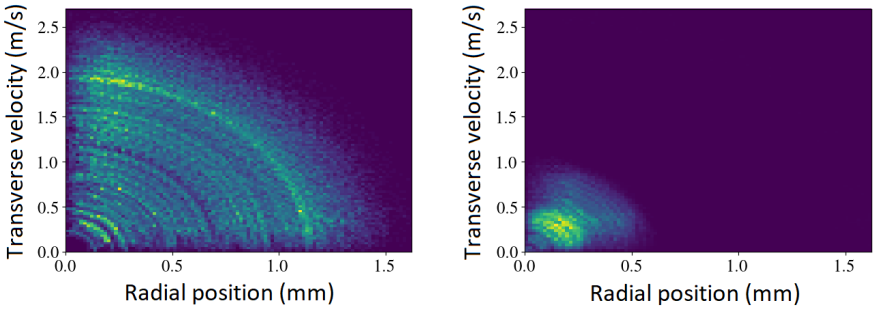

(a) (b)

Figure 36: A 2D histogram that plots positions and velocities traced out by accepted molecules within the decelerator (a) This is taken from figure 35a here the molecules take all kinds of trajectories. (b) Here the trajectories shown in figure 35b are plotted, it becomes clear that only a small part is filled

cluding the transverse losses. There also seems to be a difference in the optimal voltage. It has been concluded that this extrapolation is therefore not valid at these different voltages.
The extrapolation at different deceleration strengths shows a decent agreement with the experiment. There was still a small difference between the timings of the two. It was found to be too complex to extract deceleration efficiencies from the experimental data.
Opening the simulation up to a full 3D trajectory simulation introduces a modulation in the signal. This modulation was however not similar to the modulation in the experimental results. However, it still suggests a connection.
The modulation effect from the simulation was investigated. It is found that for certain longitudinal velocities the transverse losses increase heavily. This is dependant on the chosen voltage. From plotting the trajectories of these specific longitudinal velocities it became clear that accepted trajectories were very limited by the taken distance from the principal axis.
There are still some unanswered questions. As a follow-up investigation I would suggest looking for a certain oscillation frequency which would be dependant on the transverse trapping potential.

Appendices

A Polyatomic molecules

This appendix was written as a first exploration for a plan to use polyatomic molecules for an eEDM measurement. Poly-atomic molecules are molecules consisting of three or more atoms. For a more detailed discussion regarding the use of polyatomic molecules for an eEDM measurement, see the master thesis of Steinebach [5].

A.1 Polyatomic molecules in an eEDM experiment

In previous precision experiments searching for the eEDM, diatomic molecules were used. This was done for numerous reasons and in two distinct approaches. In the ThO experiment of the ACME 2 collaboration Ω-doublets are used. Ω-doublets are two closely spaced levels which both have the same J-number, different parity and a non-zero Ω, which is the projection of the electronic angular momentum onto the internuclear axis. Their degeneracy is lifted due to a Coriolis effect [14]. Using these levels allows for full polarization and internal co-magnetometry. The amount of polarization is proportional to the sensitivity of the eEDM measurement. The internal co-magnetometry enables you to reverse the EDM interaction without changing the lab fields. This allows for a great reduction of systematic errors in the experiment. However a major drawback of using diatomic molecules with these Ω-doublets is that they can not be laser cooled efficiently.
Some other precision experiments regarding the eEDM, use diatomic molecules such as YbF and BaF, including the NL-eEDM collaboration. These molecules are laser coolable. By cooling the molecules in this way, you allow for more experimental options to increase your coherence time, which is inversely proportional to the statistical error on the eEDM measurement. However, these molecules do not have these closely spaced levels of opposite parity. Therefore you cannot fully polarize a molecule. Furthermore you need to introduce some systematic errors concerned with the rotation of certain lab fields, because you do not have the internal co-magnetometer states.
It is shown by Kozyryev and Hutzler [15] that, using polyatomic molecules, one could combine the features of both experiments. Adding another atom to the molecule allows for degenerate vibrational bending modes. The degeneracy is slightly lifted by a Coriolis interaction [16]. Using low-lying excited vibrational states it becomes possible to exploit these nearly degenerate states in a similar way as Ω-doublets were used in some diatomic molecules. However, this angular momentum is not coupled to the electron unlike in the case with Ω-doublets. So it can be used to have full polarization in low lab fields. In addition the possibility of laser cooling is not necessarily excluded by this.

A.2 Laser cooling

In order to have a molecule that you can laser cool efficiently you need closed transition cycles. Highly diagonal Franck Condon factors(FCF) are to a certain extent an excellent indicator for closed cycle. We know that for highly polar diatomic molecules such as SrF and BaF there exist these good FCfs. According to Berger [17], it is possible for such diatomic molecules to replace the fluorine by functional groups such as OH or CH_3 without necessarily losing these good FCF.
These molecules also benefit from the fact that their orbitals are around the metal atom and not on the bonding between the atoms, therefore being less affected by certain excitation's.
Berger also points out that although these are all good arguments for expecting good FCF, there are also some specific effects that could disturb this, such as: Renner-Teller and Jahn-Teller effects. That is a reason why MgOH is not efficiently laser coolable.
Although it has been stated that it is rather hard to calculate the FCF, it should be possible to make some rough selection using the excellent calculations techniques available nowadays, and then consider only a few molecules for further investigation.

A.3 Effective electric field

The effective electric field, E_{eff} is a relevant parameter for the eEDM measurement as is shown in equation 1. Via the same reasoning as given in section A.2, it is predicted that the E_{eff} of the polyatomic molecules should be similar to its diatomic counterpart. The group of Borschevsky [18], demonstrated that this is indeed the case for BaOH and YbOH. Using computational methods they found that the value for E_{eff} of BaoH and YbOH are within a 1.5% difference of their diatomic counterpart e.g. BaF and YbF respectively.

A.4 Different poly-atomic molecules

SrOH

SrOH has been laser cooled by the group of Kozyryev [19]. A Sisyphus cooling scheme as shown by figure 37 was used. In this experiment the temperature in the transverse direction (in one dimension) was lowered from 50 mK to 1 mK. The molecules orginated from a cryogenic buffer-gas beam. The beam was created using laser ablation of $Sr(OH)_2$, which then produces SrOH. These molecules are in turn entrained by helium gas. When the molecules leave the source they have a transverse temperature of $\sim$50 mK .
Sisyphus cooling was used rather than a Doppler cooling scheme due to the fact that this is a more efficient technique. Therefore it requires fewer photon scatters which could possibly lead to losses to other states. In the end a transverse temperature of $\sim$2 mK was reached. Which is still an order of magnitude above the Doppler limit of $\sim$200 ηK.

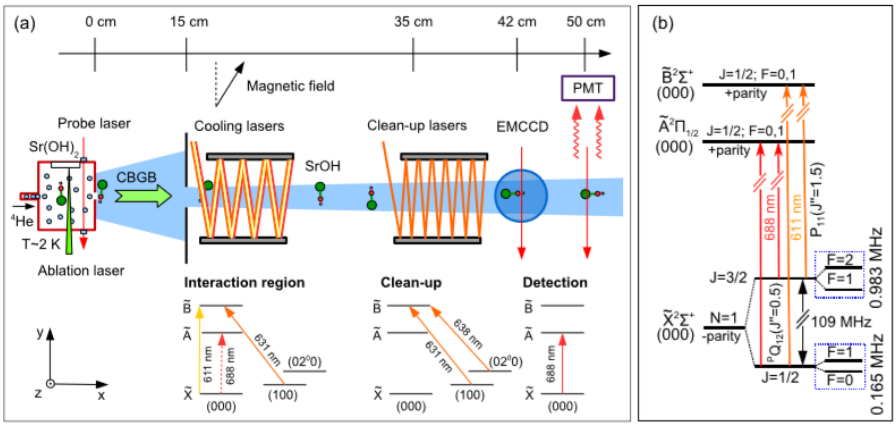

Figure 37: The cooling scheme that Kozyryev used on SrOH

The laser schemes are shown in figure 37B. Two different schemes were used. Cooling with a $\tilde{X}$-$\tilde{A}$ transition which was found to be less effective than with the $\tilde{X}$-$\tilde{B}$ transition.
Back in 1992 Steimle already created SrOH using laser ablation on a Sr target, and by letting this metallic vapor react with H_2O_2 [20].

YbOH

Kozyryev also describes a possible cooling scheme for YbOH [15], as shown in figure 38. Kozyryev explicitly stresses that the results are quite generic and can be applied to molecules similar to YbOH.
Kozyryev also warns for the fact that when one is using a cold buffer gas beam then your molecular beam can become so cold that most of the molecules are in the (000) vibrational state and therefore need punping to the (01^10) excited bending mode to preform the eEDM measurement.
YbOH was created by the group of Coxon [21]. This was done by letting Yb metal vapor react with H_2O_2. The Yb vapour is coming from a Broida-type oven, and would therefore give you molecules that would be too hot, so it would be useful to investigate a laser ablation option.

CaOH

The group of Berger has looked into the theoretical possibilities to laser cool poly-atomic molecules, [17]. In this article it is advocated that their approach to CaOH is very general and applicable to many systems like that. Their calculations are shown in figure 39. Back in 1992, Steimle created CaOH using laser ablation on a Ca target, and by letting this metallic vapor react with H_2O_2 [20].

BaOH

Production of BaOH has been achieved by the group of Steimle [22]. For their

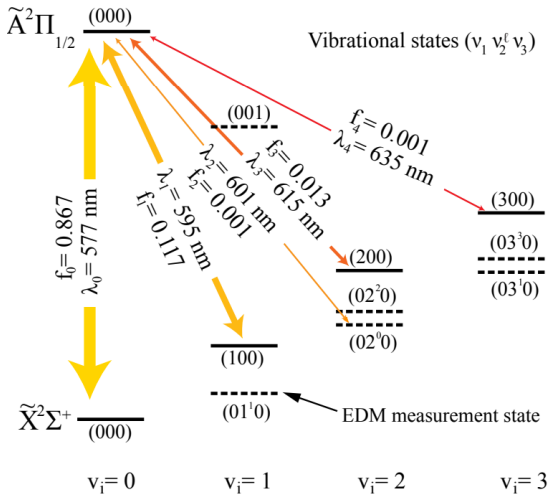

Figure 38: A possible Doppler cooling scheme for YbOH [15]

production a setup was used in which a rotating Barium rod was ablated and then was mixed with some methanol in a supersonic expansion. It is also mentioned that the setup of making BaF was rather similar as the one they used for making BaOH. In the experiment a laser induced fluorescence setup was used, which used 830 $\pm$ 10 nm indicating a excitation energy around this number. The thesis of Steinebach will go into more detail on BaOH specifically.

A.5 Conclusion

Using polyatomic molecules in the search of the eEDM is a new but promising approach, because it allows for reduction in the systematic errors via closely spaced parity doublets, and it could also allow for laser cooling.
Most of the papers regarding the eEDM measurements using these polyatomic molecules are published in the last few years. In order to know whether BaOH a is better alternative to BaF one should wait for the calculations on this molecule. All the literature points to it as a serious candidate, as it is not dismissed by the rough selection of Berger, but no concrete numbers are shown.
Furthermore, it has been shown that the creation of BaOH is feasible in a supersonic expansion. One has to use a cold buffer gas beam to do this cooling. So the possibility of creating BaOH in a cryogenic source should also be investigated. However, the fact that the group of Steimle used a similar setup for BaOH as for BaF indicates a relatively simple change in the current NL-eEDM approach, to switch towards this molecule.

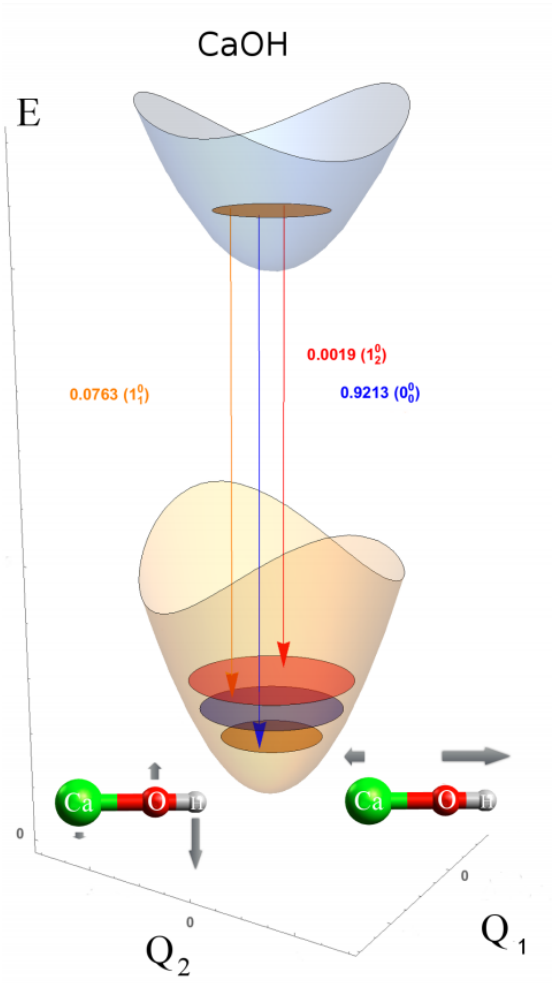

Figure 39: Some calculated FCF's of CaOH [17]. All the parameters are in arbitrary units. The transitions are indicated by : the regular number represents the excitation of the stretching mode of the first mode, the superscript indicates the vibrational number of the excited state and the subscript indicates the vibrational state of the first mode

.

B Simulation code for misalignment between the electrodes in the transverse plane

```
# H.H. Makaske 29/7/19

# The function Ringsaccept Takes initial points and a deviation
# and returns an efficiency
import numpy as np
from random import *

def RingsAccept(ringdeviation, X_list, Y_list):

  Num_accepted = 0
  X_acc = []
  Y_acc = []
  #Simulate all the x and y centres of the rings
  Centre_of_ringX = np.random.normal(0, ringdeviation, 7)
  Centre_of_ringY = np.random.normal(0, ringdeviation, 7)

  # Checking which intial points fall withing the central ring
  for entries in range(len(X_list)):
    X_point = X_list[entries]
    Y_point = Y_list[entries]
      R = np.sqrt(X_point**2 + Y_point**2)
    if R <= 2:
      X_acc.append(X_point)
      Y_acc.append(Y_point)
      Num_accepted = Num_accepted + 1
  Initaly_accepted = len(X_acc)

  # Chechking which of the points fit within the rings with
  # a random normal centre
  for ring in range(len(Centre_of_ringX)):
    new_origX = Centre_of_ringX[ring]
    new_origY = Centre_of_ringY[ring]
    for idx in range(len((X_acc))) :
      R = np.sqrt((X_acc[idx] - new_origX) ** 2 +
                  (Y_acc[idx] - new_origY) ** 2  )
      if R > 2:
        # If the point is outside a ring, its value is set to zero
        X_acc[jj] = 0
        Y_acc[jj] = 0

  # Removing all the zeroes from the accepted array
  count = 0
  length = len(X_acc)
  while(count < length):
    if(X_acc[count] == 0):
      X_acc.remove (X_acc[i])
      length = length - 1
      continue
    count = count + 1

  #The length is equal to the points that made it to the end
  LenAccptArray = len(X_acc)
  Effeciency = LenAccptArray/float(Initaly_accepted)
```

```
  return(Effeciency)


# The function Loops is used to make multiple loops of the
# Ringaccept function and return the mean of the effeciency
# retrieved by this function
def Loops(X_list, Y_list, ringdeviation, loops):
  total = 0
  for loop in range(loops):
    Effeciency = Ringsim(ringdeviation, X_list, Y_list)
    total = total + Effeciency
  mean = total / loops
  return(mean)
```

.

.

Acknowledgement

First of all I want to thank my supervisor Steven Hoekstra, for the opportunity you gave me to be part of the NL-eEDM collaboration. Steven, you always gave me the feeling that I was really part of the group. And I wish you and the rest of the collaboration good luck with the hunt on the eEDM.
I would like to thank the people who helped me during the reassembly of the decelerator. Leo, thank you for all the patience that you showed. I always had a lot of fun working with you. Mairéad, it was a pleasure working together.
Furthermore I want to thank Parul, Yanning and Kevin for the hard work to make the coupling of the cryo source with the decelerator, and supplying me with the experimental data for my thesis.
Of course I would like to thank my personal English corrector. Ginny, I really appreciate the help you gave me during the my last weeks.
I also want give a shout-out to Rutger for the fruitful discussion regarding the cryogenic source.
This acknowledgement section would not be complete without mentioning my personal tech support, Kees and Mark. I always loved your excellent coffee and the good table tennis matches.
I wish everyone at the VSI the best,
Hidde

References

[1] Ed Hinds and Ben Sauer. Electron dipole moments. *Physics World*, 10(4):37–40, apr 1997.

[2] V.Ang D. G. DeMille D. Doyle J. M. Gabrielse G. Haefner J. Hutzler N. R. Lasner Z. Meisenhelder C. O'Leary B. R. Panda C. D. West A. D. West E. P. Wu X. ACME Collaboration, Andreev. Improved limit on the electric dipole moment of the electron. 562, jan 2018.

[3] E A Hinds. Testing time reversal symmetry using molecules. *Physica Scripta*, T70:34–41, jan 1997.

[4] Parul Aggarwal, Hendrick L. Bethlem, Anastasia Borschevsky, Malika Denis, Kevin Esajas, Pi A. B. Haase, Yongliang Hao, Steven Hoekstra, Klaus Jungmann, Thomas B. Meijknecht, Maarten C. Mooij, Rob G. E. Timmermans, Wim Ubachs, Lorenz Willmann, and Artem Zapara. Measuring the electric dipole moment of the electron in BaF. *European Physical Journal D*, 72(11):197, Nov 2018.

[5] Kees Steinebach. Master thesis (university of groningen). in preparation.

[6] C. J. Foot. *Atomic Physics*. Number Vol. 7 in Oxford Master Series in Physics. OUP Oxford, 2005.

[7] R. V. Krems. *Molecules in electromagnetic fields : from ultracold physics to controlled chemistry*. John Wiley & Sons, 2018.

[8] Artem Zapara. *Dynamics of molecular beams in a traveling-wave Stark decelerator*. PhD thesis, University of Groningen, 2019.

[9] Joost Elbert van den Berg. *Traveling-wave Stark deceleration of SrF molecules*. PhD thesis, University of Groningen, 2015.

[10] Mairéad O'Shea Scanlan. Alignment and assembly of a traveling-wave stark decelerator. 2019.

[11] J. T. Muller. Simulation of electric fields and molecular motion in a traveling-wave stark decelerator. 2017.

[12] Rutger Hof. Master thesis (university of groningen). in preparation.

[13] Nicholas R. Hutzler, Hsin-I Lu, and John M. Doyle. The Buffer Gas Beam: An Intense, Cold, and Slow Source for Atoms and Molecules. *arXiv e-prints*, page arXiv:1111.2841, Nov 2011.

[14] J Baron, W C Campbell, D DeMille, J M Doyle, G Gabrielse, Y V Gurevich, P W Hess, N R Hutzler, E Kirilov, I Kozyryev, B R O'Leary, C D Panda, M F Parsons, B Spaun, A C Vutha, A D West, E P West, and ACME Collaboration. Methods, analysis, and the treatment of systematic errors for the electron electric dipole moment search in thorium monoxide. *New Journal of Physics*, 19(7):073029, jul 2017.

[15] Ivan Kozyryev and Nicholas R. Hutzler. Precision measurement of time-reversal symmetry violation with laser-cooled polyatomic molecules. *Phys. Rev. Lett.*, 119:133002, Sep 2017.

[16] Harald H. Nielsen and Wave H. Shaffer. A note concerning l-type doubling in linear polyatomic molecules. *The Journal of Chemical Physics*, 11(3):140–144, 1943.

[17] Timur A. Isaev and Robert Berger. Polyatomic Candidates for Cooling of Molecules with Lasers from Simple Theoretical Concepts. *Phys. Rev. Lett.*, 116:063006, February 2016.

[18] Malika Denis, Pi A. B. Haase, Rob G. E. Timmermans, Ephraim Eliav, Nicholas R. Hutzler, and Anastasia Borschevsky. Enhancement factor for the electric dipole moment of the electron in the baoh and yboh molecules. *Physical Review A*, 99(4), Apr 2019.

[19] Ivan Kozyryev, Louis Baum, Kyle Matsuda, Benjamin L. Augenbraun, Loic Anderegg, Alexander P. Sedlack, and John M. Doyle. Sisyphus laser cooling of a polyatomic molecule. *Phys. Rev. Lett.*, 118:173201, Apr 2017.

[20] T. C. Steimle, D. A. Fletcher, K. Y. Jung, and C. T. Scurlock. A supersonic molecular beam optical stark study of caoh and sroh. *The Journal of Chemical Physics*, 96(4):2556–2564, 1992.

[21] Todd C. Melville and John A. Coxon. The visible laser excitation spectrum of yboh. *The Journal of Chemical Physics*, 115(15):6974–6978, 2001.

[22] Sarah E. Frey and Timothy C. Steimle. Optical stark spectroscopy of the ((check .bib file)) (000) system of barium monohydroxide, baoh. *Chemical Physics Letters*, 512(1):21 – 24, 2011.